# Modeling of Cylindrical Pin-Fin Heat Sinks for Electronic Packaging

Waqar Ahmed Khan, J. Richard Culham, *Member, IEEE*, and M. Michael Yovanovich

***Abstract*—Analytical models are developed for determining heat transfer from in-line and staggered pin-fin heat sinks used in electronic packaging applications. The heat transfer coefficient for the heat sink and the average temperature of the fluid inside the heat sink are obtained from an energy balance over a control volume. In addition, friction coefficient models for both arrangements are developed from published data. The effects of thermal conductivity on the thermal performance are also examined. All models can be applied over a wide range of heat sink parameters and are suitable for use in the design of pin-fin heat sinks. The present models are in good agreement for high Reynolds numbers with existing experimental/numerical data.**

***Index Terms*—Heat transfer, pin-fin heat sinks.**

## NOMENCLATURE

| | |
|---|---|
| $A$ | area $[\mathrm{m}^2]$. |
| $c_p$ | Specific heat of fluid, $[\mathrm{J/kg \cdot K}]$. |
| $D$ | Pin diameter [m]. |
| $f$ | Friction factor. |
| $H$ | Pin height [m]. |
| $h$ | Heat transfer coefficient $[\mathrm{W/m^2K}]$. |
| $K_1$ | Correction factor. |
| $k$ | Thermal conductivity [W/mK]. |
| $k_c$ | Coefficient of contraction. |
| $k_e$ | Coefficient of expansion. |
| $L$ | Length of heat sink in flow direction [m]. |
| $m$ | Fin performance parameter $[\mathrm{m}^{-1}]$. |
| $\dot{m}$ | Mass flow rate of air [kg/s]. |
| $N$ | Total number of pins in heat sink $\equiv N_T N_L$. |
| $N_L$ | Number of rows in streamwise direction. |
| $N_T$ | Number of rows in spanwise direction. |
| $Nu_D$ | Nusselt number based on pin diameter. |
| $\mathrm{Pr}$ | Prandtl number $\equiv c_p \mu/k$. |
| $Q$ | Heat flow rate [W]. |
| $R$ | Resistance $[^\circ\mathrm{C/W}]$. |
| $\mathrm{Re}_D$ | Reynolds number based on maximum velocity between pin-fins $\equiv DU_{\max}/\nu$. |
| $\mathcal{S}_D$ | Dimensionless diagonal pitch $\equiv S_D/D$. |
| $\mathcal{S}_L$ | Dimensionless streamwise pitch $\equiv S_L/D$. |
| $\mathcal{S}_T$ | Dimensionless spanwise pitch $\equiv S_T/D$. |
| $S_D$ | Diagonal pitch [m]. |
| $S_L$ | Pin spacing in streamwise direction [m]. |
| $S_T$ | Pin spacing in spanwise direction [m]. |
| $T$ | Absolute temperature [K]. |
| $t$ | Thickness [m]. |
| $U$ | Velocity of air [m/s]. |
| $W$ | Width of heat sink [m]. |

Greek

| | |
|---|---|
| $\Delta P$ | Pressure drop [Pa]. |
| $\gamma$ | Slenderness ratio $\equiv H/D$. |
| $\mu$ | Absolute viscosity of fluid [kg/ms]. |
| $\nu$ | Kinematic viscosity of fluid $[\mathrm{m}^2/\mathrm{s}]$. |
| $\rho$ | Fluid density $[\mathrm{kg/m}^3]$. |

Subscripts

| | |
|---|---|
| app | Approach. |
| $a$ | Ambient. |
| $b$ | Exposed surface of base plate. |
| max | Max. |
| $w$ | Wall. |
| $f$ | Fluid. |
| fin | Single fin. |
| $hs$ | Heat sink. |
| $m$ | Bulk material. |

Manuscript received June 9, 2005; revised September 6, 2007. Current version published September 17, 2008. This work was supported by the Natural Sciences and Engineering Research Council of Canada and the Center for Microelectronics Assembly and Packaging. This work was recommended for publication by Associate Editor D. Donahoe upon evaluation of the reviewers comments.

W. A. Khan is with the Department of Engineering Sciences, National University of Sciences and Technology, PN Engineering College, PNS Jauhar, Karachi-75350, Pakistan (e-mail: whkhan_2000@yahoo.com).

J. R. Culham and M. M. Yovanovich are with the Microelectronics Heat Transfer Laboratory, Department of Mechanical Engineering, University of Waterloo, Waterloo, ON N2L 3G1 Canada.

Color versions of one or more of the figures in this paper are available online at http://ieeexplore.ieee.org.

Digital Object Identifier 10.1109/TCAPT.2008.2002554

## I. INTRODUCTION

HEAT sinks are the most common thermal management hardware used in micro- and opto-electronics. They improve the thermal control of electronic components, assemblies, and modules by enhancing their surface area through the use of fins. Applications utilizing pin-fin heat sinks for cooling of electronics have increased significantly during the last few decades

due to an increase in heat flux densities and product miniaturization. To the author's knowledge, no analytical work exists for the fluid friction for pin-fin heat sinks. However, many experimental/numerical studies regarding flow across tube banks exists in literature. Due to similarities between the geometry of a heat exchanger tube bundle and pin-fin arrays, previous work related to tube banks provides some guidance in modeling fluid flow in pin-fin heat sinks.

### A. Previous Work

Chilton and Genereaux [1], Grimison [2], Jakob [3], and Gunter and Shaw [4] reviewed the existing data obtained by a number of authors including Bergelin et. al [5], Norris and Spofford [6], Huge [7], Pierson [8], and Wallis and White [9] on the pressure drop across tube banks and proposed different correlations of friction factors for both in-line and staggered arrangements in terms of Reynolds numbers. Žukauskas and Ulinskas [10] recommended more than 30 empirical correlations for friction factors based on arrangement, Reynolds number and longitudinal and transverse pitches. In this study, these correlations are fitted to give simple correlations for each arrangement in terms of $\mathcal{S}_T$, $\mathcal{S}_L$, and $\mathrm{Re}_D$.

Dvinsky *et al.* [11], Jung and Maveety [12], You and Chang [13], Wang and Sangani [14], and Wung and Chen [15] performed numerical studies to model the heat transfer characteristics of pin-fin array heat exchangers. Some authors proposed Nusselt number correlations for a limited range of configurations and Reynolds numbers.

Tahat *et al.* [16], [17], Maudgal and Sunderland [18], Wirtz *et al.* [19], Babus'Haq *et al.* [20], Azar and Mandrone [21], and Minakami and Iwasaki [22] performed experimental studies and proposed empirical correlations. Van Fossen [23] and Metzger *et al.* [24]–[26] have done similar but independent studies of short pin-fin arrays with various aspect ratios and spacings for the staggered array. Armstrong and Winstanley [27] presented a review of works specifically on short pin fin arrays. They showed that not only is the existence of an active bounding wall a significant departure from the classical tube bundle situations, but also that the heat transfer from the pins themselves is lower than from long pin fins/cylinders. Hamilton *et al.* [28] used a 3-D finite element based numerical simulation to model the heat transfer characteristics of a staggered short pin-fin array heat exchanger. The simulation was validated against available experimental data, and then used to estimate overall array averaged heat transfer coefficient and pressure drop for various pin-fin configurations and Reynolds numbers. They proposed a correlation similar in form as by Grimisom [2] and Žukauskas and Ulinskas [10] for a limited range of configurations and Reynolds numbers. Their correlation works only for $3500 < \mathrm{Re}_{D\,\max} < 14000$.

Several other empirical models of heat transfer from tube banks in crossflow have also been reported in the literature. Grimisom [2] and Žukauskas and Ulinskas [10] are the main contributors in this regard. Their models are available in tabular form in many heat transfer text books (Holman [29], Kreith [30] and Incropera and DeWitt [31]. It is important to note that all those models were developed for a specific fluid, longitudinal and transverse pitches, Reynolds and Prandtl numbers. The user can not extrapolate those correlations over a wide range of operating conditions often found in existing heat exchangers. In order to avoid these problems new comprehensive models are developed that can be used for a wide range of parameters discussed above. In developing these models, it is assumed that the flow is steady, laminar, and fully developed.

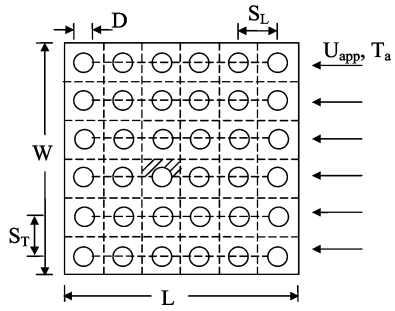


Fig. 1. Schematic of in-line arrangement.

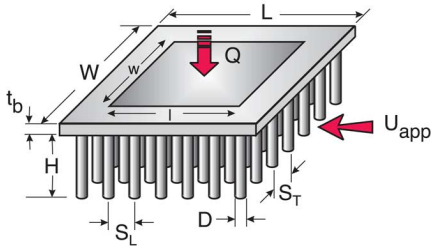


Fig. 2. Geometry of in-line pin-fin heat sink.

## II. Analysis

### A. Geometry

In pin-fin heat sinks, arrays of pin-fins are arranged in an in-line or staggered manner as shown in Figs. 1 and 2. The pins are attached to a common base and the geometry of the array is determined by the pin dimensions, number of pins and pin arrangement.

The geometry of an in-line pin-fin heat sink is shown in Fig. 2. The dimensions of the baseplate are $L \times W \times t_b$, where $L$ is the length in the streamwise direction, $W$ is the width, and $t_b$ is the thickness. Each pin fin has diameter $D$ and height $H$. The longitudinal and transverse pitches are $S_L$ and $S_T$ respectively. The approach velocity of the air is $U_{\mathrm{app}}$. The direction of the flow is parallel to the $x$-axis. The baseplate is kept at constant temperature $\overline{T}_b$ and the top surface $(y = H)$ of the pins is adiabatic. The average local wall temperature of the pin surface is $\overline{T}_w(x)$. The bottom surface $(y = 0)$ of the heat sink is kept at constant temperature $T_b$. It is assumed that the heat sink is fully shrouded.

It is assumed that the fluid temperature is averaged over the height of the heat sink, with $\overline{T}_f = \overline{T}_f(x)$, so the fluid temperature $\overline{T}_f(x)$ is the bulk mean fluid temperature. Fully developed heat and fluid flow are assumed in the analysis, and the thermophysical properties are taken to be temperature independent.

### B. Reference Velocity

The mean velocity in the minimum free cross section between two rows, $U_{\max}$, is used as a reference velocity in the calcula-

tions of fluid flow and heat transfer for both types of arrangements, and is given by

$$U_{\max} = \max\left(\frac{\mathcal{S}_T}{\mathcal{S}_T - 1}U_{\text{app}}, \frac{\mathcal{S}_T}{\mathcal{S}_D - 1}U_{\text{app}}\right) \tag{1}$$

where $U_{\text{app}}$ is the approach velocity, $\mathcal{S}_L$, and $\mathcal{S}_T$ are the dimensionless longitudinal and transverse pitches, and $\mathcal{S}_D = \sqrt{\mathcal{S}_L^2 + (\mathcal{S}_T/2)^2}$ is the dimensionless diagonal pitch in the case of a staggered arrangement. The average heat transfer coefficient of a single pin-fin taken from the first row of an in-line or staggered PFHS can be determined by an integral method of boundary layer analysis. In this study, the Von Karman-Pohlhausen integral method is used to solve the momentum and the energy equations for the isothermal boundary condition. A fourth-order velocity profile in the hydrodynamic boundary layer and a third-order temperature profile in the thermal boundary layer are used.

You and Chang [13] found numerically that the flow inside the pin-fin channel reaches the fully developed thermal state in the early downstream region whereas Žukauskas [34] showed experimentally that the heat transfer becomes stable from the third or fourth row depending upon the Reynolds number. Depending on this information, a control volume (CV) is selected from the fourth row as a typical cell (Fig. 3) to study the heat transfer from an in-line or staggered tube bank. The width of the control volume is taken as unity for convenience and the length and height, in dimensionless form, are taken as $\mathcal{S}_L$ and $\mathcal{S}_T/2$ ($\equiv S_T/2D$) respectively. Because the flow is symmetrical about the horizontal center-line, the solution has been obtained for half of the flow domain, i.e., for ABCEFG in Fig. 3. The control volume surface can be regarded as impermeable, adiabatic and shear free (no mass transfer and shear work transfer across the boundary). The heat transfer between the tube and stream is $Q$ and the wall temperature is $T_w$. The governing equations, velocity and temperature distributions for the CV inside the boundary layer are the same as described by Khan [35]. A fourth-order velocity profile in the hydrodynamic boundary layer and a third-order temperature profile in the thermal boundary layer are used.

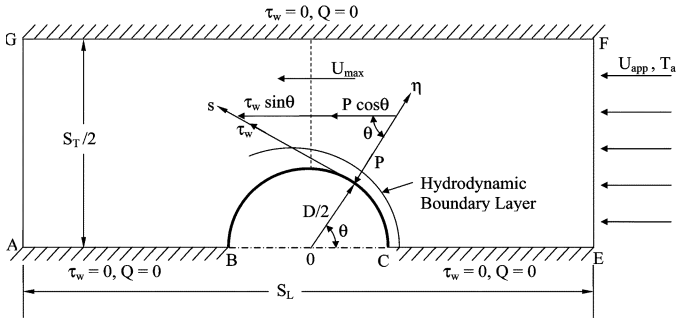


Fig. 3. Control volume for prediction of heat transfer from PFHS.

The potential flow velocity outside the boundary layer was obtained by using complex variable theory and following Suh *et al.* [36] it can be written as:

$$U = U_{\max} f(\theta) \tag{2}$$

where

$$f(\theta) = \sin\theta - 2\sin^2\left(\frac{\pi}{2\mathcal{S}_L}\right) \times \left\{ \frac{\cosh\left(\frac{\pi}{\mathcal{S}_L}\sin\theta\right)\sin\theta}{\cosh\left(\frac{\pi}{\mathcal{S}_L}\sin\theta\right) - \cos\left(\frac{\pi}{\mathcal{S}_L}\cos\theta\right)} + \sinh\left(\frac{\pi}{\mathcal{S}_L}\sin\theta\right) \times \frac{\sinh\left(\frac{\pi}{\mathcal{S}_L}\sin\theta\right)\sin\theta + \cos\theta\sin\left(\frac{\pi}{\mathcal{S}_L}\cos\theta\right)}{\left[\cosh\left(\frac{\pi}{\mathcal{S}_L}\sin\theta\right) - \cos\left(\frac{\pi}{\mathcal{S}_L}\cos\theta\right)\right]^2} \right\} \tag{3}$$

for an in-line arrangement and see (4), shown at the bottom of the page, for the staggered arrangement.

$$f(\theta) = \sin\theta - 2\sin^2\left(\frac{\pi}{4\mathcal{S}_L}\right) \times \left\{ \frac{\cosh\left(\frac{\pi\sin\theta}{2\mathcal{S}_L}\right)\sin\theta}{\cosh\left(\frac{\pi\sin\theta}{2\mathcal{S}_L}\right) - \cos\left(\frac{\pi\cos\theta}{2\mathcal{S}_L}\right)} - \sinh\left(\frac{\pi\sin\theta}{2\mathcal{S}_L}\right) \times \frac{\sinh\left(\frac{\pi\sin\theta}{2\mathcal{S}_L}\right)\sin\theta + \sin\left(\frac{\pi\cos\theta}{2\mathcal{S}_L}\right)\cos\theta}{\left[\cosh\left(\frac{\pi\sin\theta}{2\mathcal{S}_L}\right) - \cos\left(\frac{\pi\cos\theta}{2\mathcal{S}_L}\right)\right]^2} + \frac{\cosh\left(\pi\frac{\sin\theta - 2\mathcal{S}_T}{2\mathcal{S}_L}\right)\sin\theta}{\cosh\left(\pi\frac{\sin\theta - 2\mathcal{S}_T}{2\mathcal{S}_L}\right) - \cos\left(\pi\frac{\cos\theta - 2\mathcal{S}_L}{2\mathcal{S}_L}\right)} - \sinh\left(\pi\frac{\sin\theta - 2\mathcal{S}_T}{2\mathcal{S}_L}\right) \frac{\sinh\left(\pi\frac{\sin\theta - 2\mathcal{S}_T}{2\mathcal{S}_L}\right)\sin\theta + \sin\left(\pi\frac{\cos\theta - 2\mathcal{S}_L}{2\mathcal{S}_L}\right)\cos\theta}{\left[\cosh\left(\pi\frac{\sin\theta - 2\mathcal{S}_T}{2\mathcal{S}_L}\right) - \cos\left(\pi\frac{\cos\theta - 2\mathcal{S}_L}{2\mathcal{S}_L}\right)\right]^2} \right\} \tag{4}$$

### C. Boundary Conditions

1) On the curved surfaces of the pin-fin

$$u = 0 \quad v = 0 \text{ and } T = T_w.$$

2) Along the top and bottom of the control volume and on the side-wall regions between pin-fins

$$v = 0 \quad \tau_w = 0 \text{ and } Q = 0.$$

3) At the entrance of the CV

$$u = U_{\text{app}} \text{ and } T = T_a.$$

4) At the exit of the CV

$$T = T_0.$$

In reality, the velocity $U_{\text{app}}$ is not uniform at the EF plane for any arrangement. This velocity profile depends on many factors including Reynolds number, longitudinal and transverse pitches as well as the method of tubes arrangement. These velocity profiles are presented in graphical form by Žukauskas and Ulinskas [10] for some specific cases and in such case it is not possible to reproduce graphical information in terms of the above mentioned factors. In order to proceed analytically, it is therefore assumed that the approach velocity is uniform. Due to this assumption, higher (around 12%) local heat transfer coefficients are obtained than the experimental/numerical values. In averaging the heat transfer coefficients over the entire surface, they are reduced to some extent.

Assuming the presence of a thin thermal boundary layer $\delta_T$ along the tube surface in the CV, the energy integral equation for the isothermal boundary condition can be written as

$$\frac{d}{ds}\int_0^{\delta_T}(T - T_\infty)u\,d\eta = -\alpha\left.\frac{\partial T}{\partial \eta}\right|_{\eta=0}. \tag{5}$$

Using a fourth-order velocity profile and a third-order temperature profile that satisfy all the boundary conditions (Khan *et al.* [37]) and assuming $\zeta = \delta_T/\delta < 1$ for $\text{Pr} \geq 1$, (5) can be integrated to give

$$\delta_T \frac{d}{ds}\left[U(s)\delta_T\zeta(\lambda + 12)\right] = 90\alpha \tag{6}$$

where $U(s)$ is the potential flow velocity outside the boundary layer, and $\lambda$ is the pressure gradient parameter obtained from the momentum integral equation and the definition of momentum boundary layer thickness. The values of $\lambda$ are obtained corresponding to each position along the tube surface and are fitted by the least squares method and given by

$$\lambda = 7.36 - 3.74\theta + 27.95\theta^2 - 96.64\theta^3 + 157.83\theta^4 - 135.87\theta^5 + 58.65\theta^6 - 10.10\theta^7. \tag{7}$$

Integrating (6) with respect to $s$, one can obtain local thermal boundary layer thicknesses

$$\left(\frac{\delta_T(\theta)}{D}\right)\cdot \text{Re}_D^{1/2}Pr^{1/3} = \sqrt[3]{\frac{90I_1}{(\lambda+12)^2 f(\theta)^2}\sqrt{\frac{\lambda}{2g(\theta)}}} \tag{8}$$

where $g(\theta)$ is the derivative of the function $f(\theta)$ with respect to $\theta$ and $I_1$ is given by

$$I_1 = \int_0^\theta f(\theta)(\lambda + 12)d\theta. \tag{9}$$

The local heat transfer coefficient can be written as

$$h(\theta) = \frac{3k_f}{2\delta_T}. \tag{10}$$

Thus, the dimensionless local heat transfer coefficient can be written as

$$\frac{Nu_{Df}(\theta)|_{\text{isothermal}}}{\text{Re}_D^{1/2}Pr^{1/3}} = \frac{3}{2}\sqrt[3]{\frac{(\lambda+12)^2 f(\theta)^2}{90I_1}\sqrt{\frac{2g(\theta)}{\lambda}}}. \tag{11}$$

The average heat transfer coefficient is defined as

$$\begin{aligned} h &= \frac{1}{\pi}\int_0^\pi h(\theta)d\theta \\ &= \frac{1}{\pi}\int_0^{\theta_s} h(\theta)\,d\theta + \frac{1}{\pi}\int_{\theta_s}^{\pi} h(\theta)\,d\theta. \end{aligned} \tag{12}$$

In dimensionless form, heat transfer coefficient can be written as

$$Nu_{Df} = \frac{hD}{k_f} = Nu_{Df1} + Nu_{Df2}. \tag{13}$$

The first term on the right hand side gives the dimensionless average heat transfer coefficient of the tube from the front stagnation point to the separation point, and can be obtained, using (11), (12), for different pitch ratios and then correlated them to obtain a single expression in terms of $\text{Re}_D$ and $Pr$ numbers for both in-line and staggered arrangements. This expression can be written as

$$Nu_{Df1} = C_2\text{Re}_D^{1/2}Pr^{1/3} \tag{14}$$

where $C_2$ is a constant which depends upon the longitudinal and transverse pitches, arrangement of the tubes, and thermal boundary conditions. For isothermal boundary condition, it is given by (15), shown at the bottom of the page. Equation (15) is valid for $1.25 \leq \mathcal{S}_L \leq 3$ and $1.25 \leq \mathcal{S}_T \leq 3$ for both arrangements (see Fig. 4).

The second term on the right hand side of (12) gives the dimensionless average heat transfer coefficient of the tube from the separation point to the rear stagnation point. The integral analysis is unable to predict these heat transfer coefficients. The

$$C_2 = \begin{cases} \frac{-.016+.6\mathcal{S}_L{}^2}{0.4+\mathcal{S}_L{}^2}, & \text{In-Line} \\ (0.588 + 0.004\mathcal{S}_T)(0.858 + 0.04\mathcal{S}_T - 0.008\mathcal{S}_T{}^2)^{1/\mathcal{S}_L}, & \text{Staggered} \end{cases} \tag{15}$$

Experiments [37], [38], [39] show that, the heat transfer from the rear portion of the cylinder increases with Reynolds numbers. From a collection of all known data, Van der Hegge Zijnen [40] demonstrated that the heat transferred from the rear portion of the cylinder to the air can be determined from

$$Nu_{Df2} = 0.001\mathrm{Re}_D. \tag{16}$$

Thus, the total heat transfer coefficient from a single tube in the first row can be written as

$$Nu_{Df} = C_2\mathrm{Re}_D^{1/2}\,\mathrm{Pr}^{1/3} + 0.001\mathrm{Re}_D. \tag{17}$$

### *D. Average Heat Transfer Coefficient for Heat Sink*

If the base temperature of the heat sink $\overline{T}_b$ is averaged and assumed to be constant, the energy balance for the control volume (Fig. 3) is

$$Q = NQ_{\mathrm{fin}} + Q_b \tag{18}$$

where

$$Q = (hA)_{hs}\theta_b \tag{19}$$
$$Q_{\mathrm{fin}} = (Ah\eta)_{\mathrm{fin}}\theta_b \tag{20}$$
$$Q_b = (hA)_b\theta_b \tag{21}$$

with

$$A_{hs} = NA_{\mathrm{fin}} + \left(LW - N\frac{\pi D^2}{4}\right) \tag{22}$$
$$A_{\mathrm{fin}} = \pi DH \tag{23}$$
$$A_b = LW - N\frac{\pi D^2}{4} \tag{24}$$
$$\eta_{\mathrm{fin}} = \frac{\tanh(mH)}{mH} \tag{25}$$
$$m = \sqrt{\frac{4h_{\mathrm{fin}}}{kD}} \tag{26}$$
$$N = N_L N_T \tag{27}$$
$$\theta_b = \overline{T}_b - T_a. \tag{28}$$

The mean heat transfer coefficients $h_{\mathrm{fin}}$ and $h_b$ for the baseplate and the pin-fin arrays are obtained by Khan [32] and are written as

$$h_b = \frac{0.75k_f}{D}\sqrt{\frac{\mathcal{S}_T - 1}{N_L\mathcal{S}_L\mathcal{S}_T}}\mathrm{Re}_D^{1/2}Pr^{1/3} \tag{29}$$
$$h_{\mathrm{fin}} = \frac{C_1k_f}{D}\mathrm{Re}_D^{1/2}Pr^{1/3} \tag{30}$$

where $C_1$ is a constant which depends upon the longitudinal and transverse pitches, arrangement of the pins, and thermal boundary conditions. For isothermal boundary condition, it is given by (31), shown at the bottom of the page. Combining (18)–(20), (21) can be solved for the average heat transfer coefficient of the heat sink

$$h_{hs} = C_2\frac{k_f}{D}\mathrm{Re}_D^{1/2}Pr^{1/3} \tag{32}$$

where $C_2$ is a constant and for both pin-fin arrangements, it is written as

$$C_2 = \frac{C_1\pi\gamma\eta_{\mathrm{fin}} + 0.75\sqrt{\frac{\mathcal{S}_T-1}{N_L\mathcal{S}_L\mathcal{S}_T}}\left(\mathcal{S}_T\mathcal{S}_L - \frac{\pi}{4}\right)}{\pi\left(\gamma - \frac{1}{4}\right) + \mathcal{S}_T\mathcal{S}_L} \tag{33}$$

and $\gamma = H/D$ is the aspect ratio of the fin. Thus the dimensionless heat transfer coefficient for the heat sink may be expressed as

$$Nu_{D_{hs}} = \frac{h_{hs}D}{k_f} = C_2\mathrm{Re}_D^{1/2}Pr^{1/3}. \tag{34}$$

### *E. Average Fluid Temperature*

An energy balance for the control volume of length $\Delta x$ (Fig. 5) gives

$$\dot{m}c_p[T_f(x+\Delta x) - T_f(x)] = dQ \tag{35}$$

where $\dot{m}$ is the mass flow rate of air and $dQ$ is the heat flow coming from the fin and the exposed (unfinned) surface of the baseplate and they are given by

$$\dot{m} = \rho U_{\mathrm{app}}N_TS_TH \tag{36}$$
$$dQ = dQ_{\mathrm{fin}} + dQ_b. \tag{37}$$

Equation (35) can be simplified and integrated to give the fluid temperature $T_f(x)$ at any position inside the heat sink

$$T_f(x) = \overline{T}_b - (\overline{T}_b - T_a)\cdot\exp\left[-\frac{(hA)_{hs}}{\dot{m}c_p}\cdot\left(\frac{x}{L}\right)\right]. \tag{38}$$

Therefore, the average fluid temperature inside the heat sink will be

$$\overline{T}_f = \overline{T}_b - (\overline{T}_b - T_a)\left[\frac{\dot{m}c_p}{(hA)_{hs}}\right]\cdot\left[1 - \exp\left(-\frac{(hA)_{hs}}{\dot{m}c_p}\right)\right]. \tag{39}$$

The air temperature leaving the heat sink can be determined from (39) by using $T_f(x) = T_0$ at $x = L$

$$T_o = \overline{T}_b - (\overline{T}_b - T_a)\cdot\exp\left[-\frac{(hA)_{hs}}{\dot{m}c_p}\right]. \tag{40}$$

$$C_1 = \begin{cases} 0.2 + \exp(-0.55\mathcal{S}_L)\mathcal{S}_T^{0.285}\mathcal{S}_L^{0.212}, & \text{In-Line Arrangement} \\ \frac{0.61\mathcal{S}_T^{0.091}\mathcal{S}_L^{0.053}}{[1-2\exp(-1.09\mathcal{S}_L)]}, & \text{Staggered Arrangement} \end{cases} \tag{31}$$

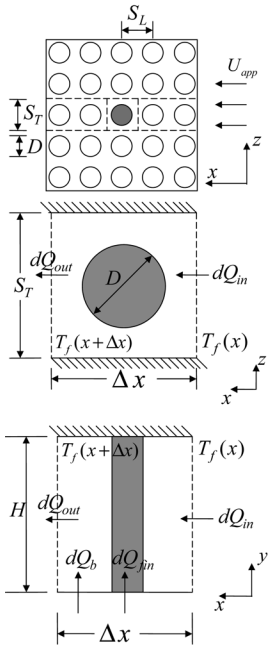


Fig. 4. Control volume for energy balance.

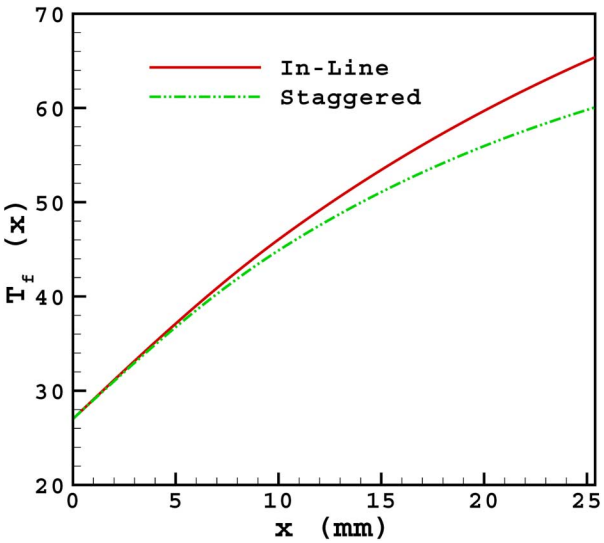


Fig. 5. Temperature distribution of air in pin-fin heat sink.

### F. Heat Sink Resistance

Assuming that the entire baseplate is fully covered with electronic components, and the fins are machined as an integral part of the baseplate, the thermal resistance of the heat sink can be written as

$$R_{th} = \frac{1}{\frac{N}{R_{\text{fin}}} + \frac{1}{R_b}} + R_m \tag{41}$$

where $N$ is the total number of pin-fins, $R_{\text{fin}}$ is the thermal resistance of the fin and is given by

$$R_{\text{fin}} = \frac{1}{(hA\eta)_{\text{fin}}} \tag{42}$$

TABLE I
DIMENSIONS USED FOR MODELING OF PIN-FIN HEAT SINKS

| Quantity | Dimension |
|---|---|
| Footprint ($mm^2$) | $25.4 \times 25.4$ |
| Heat Source Dimensions ($mm^2$) | $25.4 \times 25.4$ |
| Baseplate Thickness ($mm$) | 2 |
| Pin Diameter ($mm$) | 2 |
| Overall Height of Heat Sink ($mm$) | 12 |
| Number of Pins (In-Line) $N_T \times N_L$ | $7 \times 7$ |
| Number of Pins (Staggered) $N_T \times N_L$ | $8 \times 7$ |
| Approach Velocity ($m/s$) | 3 |
| Thermal Conductivity of Solid ($W/m \cdot K$) | 180 |
| Thermal Conductivity of Air ($W/m \cdot K$) | 0.026 |
| Density of Air ($kg/m^3$) | 1.1614 |
| Specific Heat of Air ($J/kg \cdot K$) | 1007 |
| Kinematic Viscosity ($m^2/s$) | $1.58 \times 10^{-5}$ |
| Prandtl Number (Air) | 0.71 |
| Heat Load ($W$) | 50 |
| Ambient Temperature ($^0C$) | 27 |

where $R_b$ is the thermal resistance of the exposed surface of the baseplate, i.e.,

$$R_b = \frac{1}{h_b\left(LW - N\frac{\pi D^2}{4}\right)} \tag{43}$$

and $R_m$ is the bulk resistance of the baseplate material and is given by

$$R_m = \frac{t_b}{kLW} \tag{44}$$

where $k$ is the thermal conductivity of the baseplate, $h_b$ and $h_{\text{fin}}$ are the mean heat transfer coefficients for the fin array and the baseplate and can be determined from (29) and (30), respectively.

### G. Heat Sink Pressure Drop

For a heat sink, the total pressure drop is given by

$$\Delta P_{tot} = \Delta P_{1-a} + \Delta P_{a-b} + \Delta P_{b-2} \tag{45}$$

where $\Delta P_{1-a}$ is the pressure drop due to the irreversible free expansion that always follows the abrupt contraction, $\Delta P_{a-b}$ is the pressure loss due to core friction, and $\Delta P_{b-2}$ is the pressure loss associated with the irreversible free expansion and momentum changes following an abrupt expansion. These pressure drops can be written as

$$\left.\begin{aligned} \Delta P_{1-a} &= k_c \cdot \frac{\rho U_{\max}^2}{2} \\ \Delta P_{b-2} &= k_e \cdot \frac{\rho U_{\max}^2}{2} \\ \Delta P_{a-b} &= f N_L \cdot \frac{\rho U_{\max}^2}{2} \end{aligned}\right\} \tag{46}$$

where $k_c$ and $k_e$ are the abrupt contraction and abrupt expansion coefficients, respectively, $f$ is the friction factor, and $N_L$ is the

TABLE II
RESULTS OF IN-LINE AND STAGGERED HEAT SINKS

| Quantity | In-Line | Staggered |
|---|---|---|
| Thermal Resistance ($^0C/W$) | 1.35 | 0.94 |
| Average Heat Transfer Coefficient ($W/m^2 \cdot K$) | 210.7 | 271.8 |
| Pressure Drop ($Pa$) | 78.5 | 211.9 |
| Average Fluid Temperature ($^0C$) | 48.9 | 46.8 |
| Average Baseplate Temperature ($^0C$) | 94.3 | 74.0 |
| Air Temperature Leaving Heat Sink ($^0C$) | 65.4 | 60.1 |

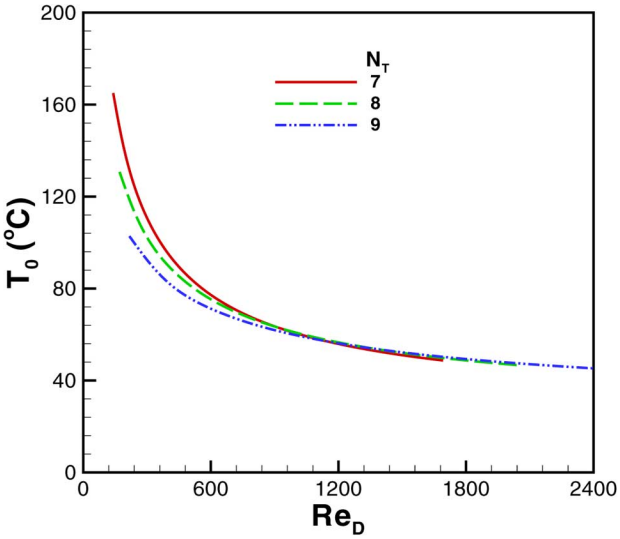


Fig. 6. Temperature of air leaving heat sink as function of $\mathrm{Re}_D$ and $N_T$.

number of pins in the longitudinal direction. The coefficients of abrupt contraction and expansion have been established graphically by Kays [33] for a number of geometries. The following correlations are derived from those graphs:

$$\left.\begin{aligned} k_c &= -0.0311\sigma^2 - .3722\sigma + 1.0676 \\ k_e &= 0.9301\sigma^2 - 2.5746\sigma + 0.973 \end{aligned}\right\} \tag{47}$$

with

$$\sigma = \frac{\mathcal{S}_T - 1}{\mathcal{S}_T}. \tag{48}$$

Žukauskas and Ulinskas [10] collected data, from a variety of sources, about friction factors for the flow through in-line and staggered arrays having many rows and plotted them in the form $Eu/K_1$ versus $\mathrm{Re}_D$, where $Eu$ is the dimensionless pressure drop and $K_1$ is a parameter accounting for geometry. They fitted

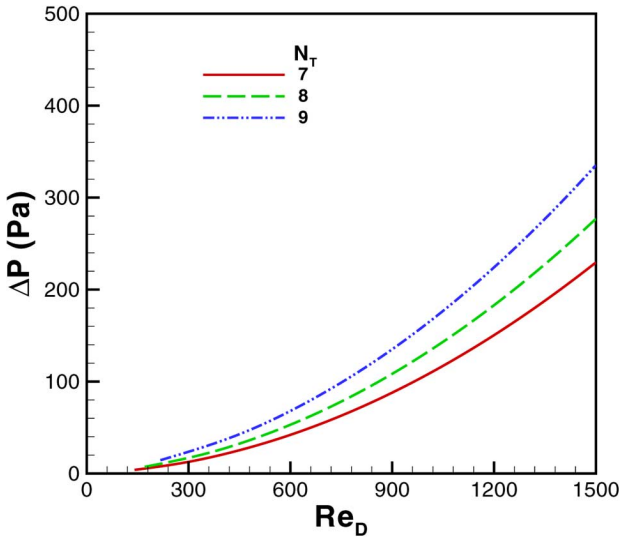


Fig. 7. Pressure drop as function of red for in-line arrangement.

these plots by inverse power series relationships and recommended several correlations depending on of $\mathcal{S}_L$, $\mathcal{S}_T$ and $\mathrm{Re}_D$. They also fitted and recommended several correlations for the correction factors for the pressure drop with small number of rows. These authors digitized all the graphical results for pressure drop and their correction factors separately and used curve expert software to develop single correlations for the friction factors and correction factors for each arrangement. These correlations can be used for $1.25 \leq \mathcal{S}_T$, $\mathcal{S}_L \leq 3.0$ and $10^3 \leq \mathrm{Re}_D \leq 2 \times 10^5$. They are given by

$$f = \begin{cases} K_1 \left[\dfrac{0.233 + 45.78}{(\mathcal{S}_T - 1)^{1.1}\mathrm{Re}_D}\right], & \text{In-Line Arrangement} \\ \dfrac{K_1 \left[\dfrac{378.6}{\mathcal{S}_T^{13.1/\mathcal{S}_T}}\right]}{\mathrm{Re}_D^{0.68/\mathcal{S}_T^{1.29}}}, & \text{Staggered Arrangement} \end{cases} \tag{49}$$

where $K_1$ is a correction factor depending upon the flow geometry and arrangement of the pins. It is given by (50), shown at the bottom of the page.

## III. RESULTS AND DISCUSSION

The dimensions given in Table I are used as the default case for the modeling of both in-line and staggered pin-fin heat sinks. The air properties are evaluated at the ambient temperature. The results obtained for both in-line and staggered arrangements are shown in Table II. It is obvious from Table II that the in-line arrangement gives higher thermal resistance and lower pressure drop than the staggered arrangement. As a result, the average heat transfer coefficient is lower and the baseplate temperature is higher for the in-line arrangement. It means that, under the

$$K_1 = \begin{cases} 1.009\left(\dfrac{\mathcal{S}_T - 1}{\mathcal{S}_L - 1}\right)^{1.09/\mathrm{Re}_D^{0.0553}}, & \text{In-Line Arrangement} \\ 1.175\left(\dfrac{\mathcal{S}_L}{\mathcal{S}_T \mathrm{Re}_D^{0.3124}}\right) + 0.5\mathrm{Re}_D^{0.0807}, & \text{Staggered Arrangement} \end{cases} \tag{50}$$

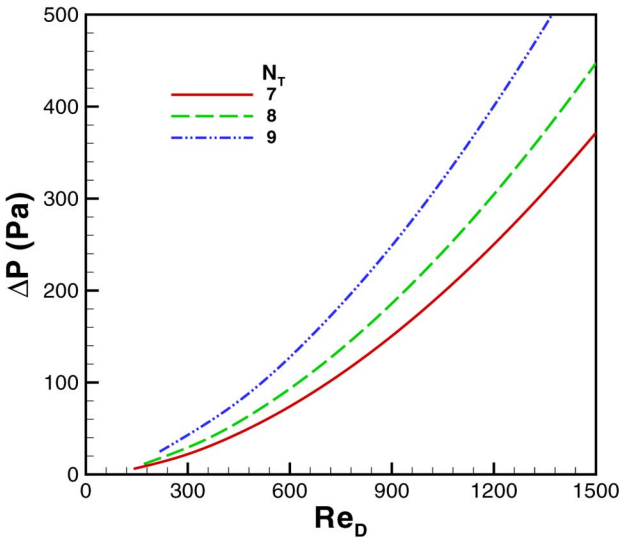


Fig. 8. Pressure drop as function of $\mathrm{Re}_D$ for staggered arrangement.

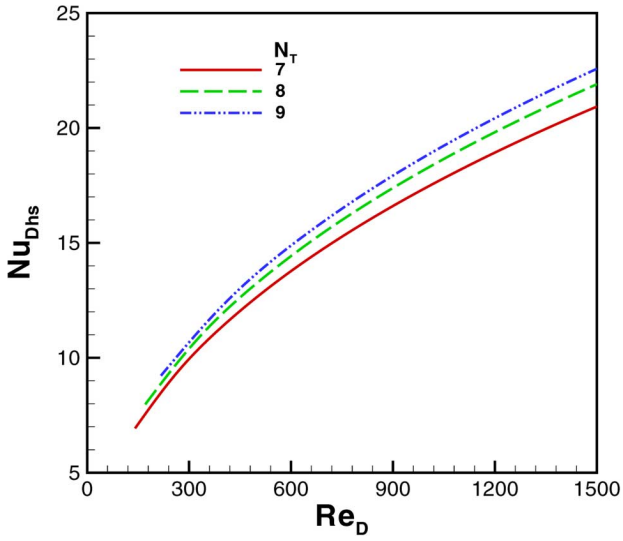


Fig. 9. Nusselt number as function of $\mathrm{Re}_D$ for in-line arrangement.

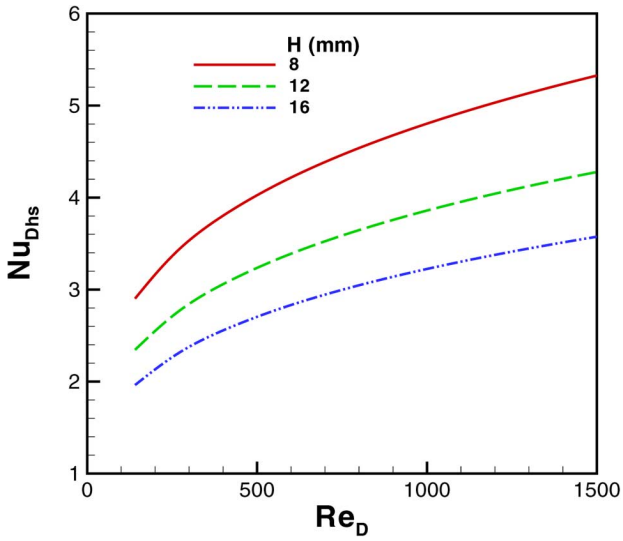


Fig. 10. Nusselt number as function of $\mathrm{Re}_D$ and $H$ for in-line arrangement.

same situation, staggered arrangement gives better thermal performance at the cost of higher pressure drop.

Fig. 5 shows the temperature distributions of air in the heat sink for both arrangements. The baseplate is kept at constant temperature $\overline{T}_b$. No appreciable effect of pin-fin arrangements on the temperature of air could be found in the entrance region. However, as the distance from the inlet increases, the in-line arrangement shows higher temperature up to the exit. This is mainly due to higher thermal resistance offered by in-line arrangement.

The variation of air temperature at the exit versus Reynolds numbers for different number of pins $N_T$ in an in-line arrangement is shown in Fig. 6. As expected, the temperature of the air leaving the heat sink decreases with increasing Reynolds number and number of transverse rows. As number of rows increases, the heat transfer surface area increases and as a result the temperature of the air decreases. The same behavior could be observed for staggered arrangement.

Fig. 7 shows the total pressure drop versus Reynolds number for different number of pins $N_T$ in an in-line arrangement. The pressure drop increases with Reynolds number and pin density. For small Reynolds numbers and pin densities, there is no appreciable change in the pressure drop. However, as the Reynolds number and the pin density increase, the difference in pressure drops increase.

Fig. 8 shows the same trend of pressure drop for different number of pins in the flow direction for staggered arrangement. In both cases, whether pin density or Reynolds number increase, hydraulic resistance increases and as a result the pressure drop increases.

Heat transfer from heat sinks depends mainly on the Reynolds number, pin arrangement, heat sink material, and properties of the incoming fluid. Dimensionless heat transfer coefficients for the heat sink are plotted in Figs. 9–12 versus Reynolds numbers for different arrangements. In Fig. 9, heat transfer coefficients versus Reynolds numbers are plotted for different pin densities. The heat transfer coefficients of the heat sink increase with the pin density. For the specified baseplate dimensions, the increase in pin density decreases the transverse as well as longitudinal pitches which increases the heat transfer.

Fig. 10 shows the variation of Nusselt number versus Reynolds numbers for different pin heights. It is evident that heat transfer decreases with the increase in pin height but increases with Reynolds numbers. With increasing number of transverse or longitudinal rows, heat transfer also increases. This is shown in Fig. 11 for staggered arrangement.

In Fig. 12, the variation of heat transfer coefficients is shown for different materials (having low thermal conductivity to high conductivity). It is clear that plastic composites ($k = 25\,\mathrm{W/m \cdot K}$) have very low heat transfer coefficients, whereas aluminum and copper ($k = 180$ and $400\ \mathrm{W/m \cdot K}$) have higher heat transfer coefficients. For higher Reynolds numbers, the difference in heat transfer between these materials is also evident. Both in-line and staggered arrangements show the same behaviour.

The comparison of the present results with the numerical data of Hamilton *et al.* [28] is presented in Fig. 13 for staggered

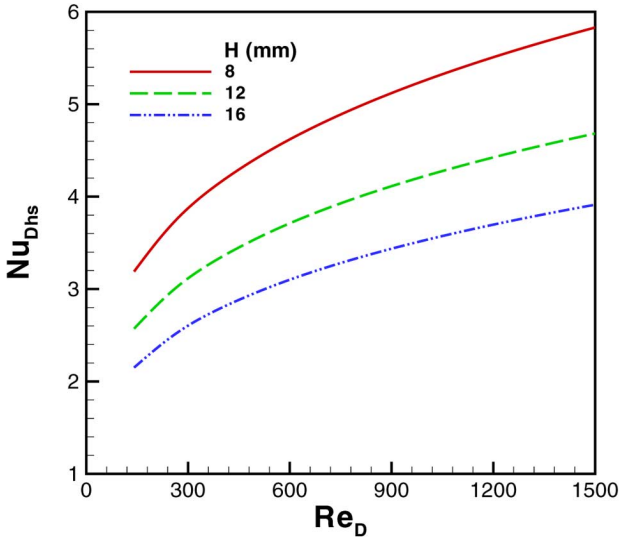


Fig. 11. Nusselt number as function of $\mathrm{Re}_D$ and $H$ for staggered arrangement.

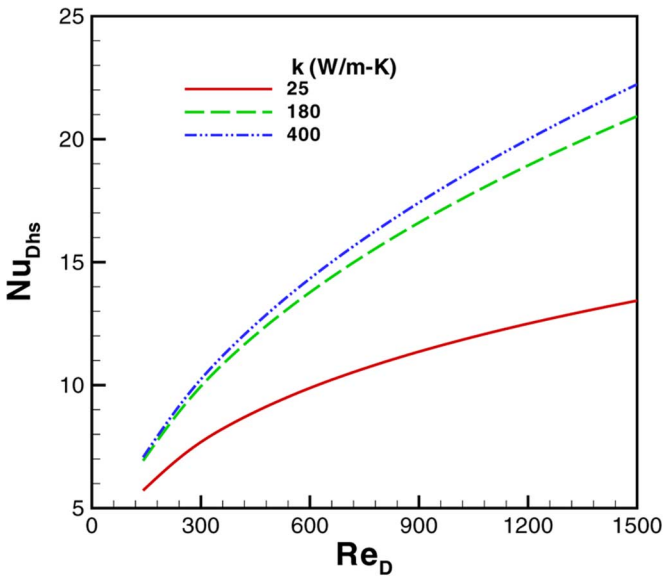


Fig. 12. Nusselt Number as function of $U_{\mathrm{app}}$ and $k$ for in-line arrangement.

arrangement. Good agreement can be noticed for high Reynold numbers.

## IV. Conclusion

Using integral method of boundary layer analysis, mathematical models are developed for friction factors and heat transfer coefficients for both in-line and staggered arrangements. The predictions of these models validate the previous experimental/numerical results and can be summarized as follows.

1) Heat transfer from and pressure drop across the heat sink increases with the increase in approach velocity, pin diameter, and number of pins. Heat transfer also increases with the thermal conductivity of the material and with the pin height.
2) In-line arrangement gives higher heat sink resistance and lower pressure drop than the staggered arrangement.

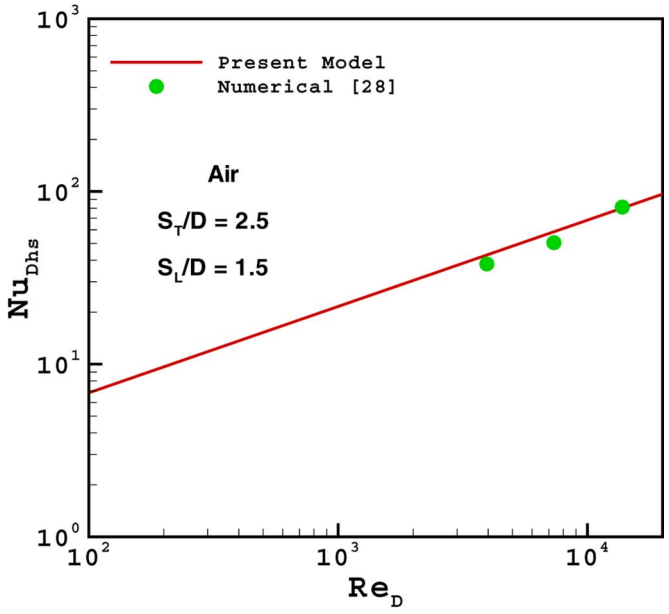


Fig. 13. Nusselt number as function of $\mathrm{Re}_D$ for $2.5 \times 1.5$ staggered arrangement.

3) Heat transfer models for in-line and staggered arrangements are suitable in designing pin-fin heat sinks.

## References

[1] T. H. Chilton and R. P. Genereaux, "Pressure drop across tube banks," *Trans. Amer. Inst. Chem. Eng.*, vol. 29, pp. 161–173, 1933.
[2] E. D. Grimison, "Correlation and utilization of new data on flow resistance and heat transfer for cross flow of gases over tube banks," *Trans. ASME*, vol. 59, pp. 583–594, 1937.
[3] M. Jakob, "Heat transfer and flow resistance in cross flow of gases over tube banks," *ASME J. Heat Transf.*, vol. 60, pp. 384–386, 1938.
[4] A. Y. Gunter and W. A. Shaw, "A general correlation of friction factors for various types of surfaces in crossflow," *Trans. ASME*, vol. 67, pp. 643–660, 1945.
[5] O. P. Bergelin, G. A. Brown, H. L. Hull, and F. W. Sullivan, "Heat transfer and fluid friction during flow across banks of tubes—III: A study of tube spacing and tube size," *ASME J. Heat Transf.*, vol. 72, pp. 881–888, 1950.
[6] R. H. Norris and W. A. Spofford, "High performance fins for heat transfer," *Trans. ASME*, vol. 64, pp. 489–496, 1942.
[7] E. C. Huge, "Experimental investigation of effects of equipment size on convection heat transfer and flow resistance in cross flow of gases over tube banks," *Trans. ASME*, vol. 59, pp. 573–581, 1937.
[8] O. L. Pierson, "Experimental investigation of the influence of tube arrangement on convection heat transfer and flow resistance in cross flow of gases over tube banks," *Trans. ASME*, vol. 59, pp. 563–572, 1937.
[9] R. P. Wallis and C. M. White, "Resistance to flow through nests of tubes," *Trans. ASME*, vol. 59, pp. 583–594, 1938.
[10] A. Žukauskas and R. Ulinskas, *Heat Transfer in Tube Banks in Crossflow*. Washington, DC: Hemisphere, 1988.
[11] A. Dvinsky, A. Bar-Cohen, and M. Strelets, "Thermofluid analysis of staggered and in-line pin fin heat sinks," in *Proc. 7th Inter Soc. Conf. Thermal Phenom.*, Las Vegas, NV, May 26, 2000, vol. 1, pp. 157–164.
[12] H. H. Jung and J. G. Maveety, "Pin fin heat sink modeling andCharacterization," in *Proc. 16th IEEE Semi-Therm Symp.*, San Jose, CA, Mar. 21, 2000, pp. 260–265.
[13] H. I. You and C. H. Chang, "Numerical prediction of heat transfer coefficient for a pin-fin channel flow," *J. Heat Transf.*, vol. 119, pp. 840–843, Nov. 1997.
[14] W. Wang and A. S. Sangani, "Nusselt number for flow perpendicular to arrays of cylinders in the limit of small Reynolds and large peclet numbers," *Phys. Fluids*, vol. 9, no. 6, pp. 1529–1539, 1997.
[15] T. S. Wung and C. J. Chen, "Finite analytic solution of convective heat transfer for tube arrays in crossflow: Part I—Flow field analysis," *ASME J. Heat Transf.*, vol. 111, pp. 633–640, Aug. 1989.
[16] M. A. Tahat, Z. H. Kodah, B. A. Jarrah, and S. D. Probert, "Heat transfer from pin-fin arrays experiencing forced convection," *Appl. Energy*, vol. 67, pp. 419–442, 2000.

[17] M. A. Tahat, R. F. Babus'Haq, and S. D. Probert, "Forced steady-state convections from pin fin arrays," *Appl. Energy*, vol. 48, pp. 335–351, 1994.
[18] V. K. Maudgal and J. E. Sunderland, "Forced convection heat transfer from staggered pin fin arrays," in *Proc. 31st Nat. Heat Transf. Conf.*, Houston, TX, Aug. 3–6, 1996, vol. 7, pp. 35–44.
[19] R. A. Wirtz, R. Sohal, and H. Wang, "Thermal performance of pin-fin fan-sink assemblies," *J. Electron. Packag.*, vol. 119, pp. 26–31, Mar. 1997.
[20] R. F. Babus'Haq, K. Akintunde, and S. D. Probert, "Thermal performance of a pin-fin assembly," *Int. J. Heat Fluid Flow*, vol. 16, no. 1, pp. 50–55, 1995.
[21] K. Azar and C. D. Mandrone, "Effect of pin fin density of the thermal performance of unshrouded pin fin heat sinks," *ASME J. Electron. Packag.*, vol. 116, pp. 306–309, 1994.
[22] K. Minakami and H. Iwasaki, "Heat-Transfer characteristics of pin-fins with in-line arrangement," *Heat Transf.—Jpn. Res.*, vol. 23, no. 3, pp. 213–228, 1994.
[23] G. J. Vanfossen, "Heat transfer coefficients for staggered arrays of short pin fins," *ASME J. Eng. Power*, vol. 104, pp. 268–274, 1982.
[24] D. E. Metzger, R. A. Berry, and J. P. Bronson, "Developing heat transfer in rectangular ducts with staggered arrays of short pin fins," *ASME J. Heat Transf.*, vol. 104, pp. 700–706, 1982.
[25] D. E. Metzger, Z. X. Fan, and W. B. Shepard, "Pressure loss and heat transfer through multiple rows of short pin fins," in *Heat Transfer*, U. Grigull, Ed. *et al.* Washington, DC: Hemisphere, 1982, vol. 3, pp. 137–142.
[26] D. E. Metzger, C. S. Fan, and S. W. Haley, "Effects of pin shape and array orientation on heat transfer and pressure loss in pin fin arrays," *ASME J. Heat Transf.*, vol. 106, pp. 252–257, 1984.
[27] J. Armstrong and D. Winstanley, "A review of staggered array pin fin heat transfer for turbine cooling applications," *ASME J. Turbomach.*, vol. 110, pp. 94–103, 1988.
[28] H. J. Hamilton, D. S. Adametz, E. K. Lind, and A. Gopinath, "Numerical analysis of the performance of a staggered cross-pin array heat exchanger," in *Proc. 8th AIAA/ASME Joint Thermophys. Heat Transf. Conf.*, St. Louis, MO, Jun. 24–26, 2002.
[29] J. P. Holman, *Heat Transfer*, 7th ed. New York: McGraw-Hill, 1992, pp. 307–310.
[30] F. Kreith and M. S. Bohn, *Principles of Heat Transfer*, 5th ed. New York: West Publishing, 1993, pp. 469–485.
[31] F. P. Incropera and D. P. DeWitt, *Introduction to Heat Transfer*. New York: Wiley, 2002.
[32] W. A. Khan, "Modeling of Fluid Flow and Heat Transfer for Optimization of Pin-Fin Heat Sinks," Ph.D. dissertation, Dept. Mech. Eng., Univ. Waterloo, Waterloo, ON, Canada, 2004.
[33] W. M. Kays, "Loss coefficients for abrupt changes in flow cross section with low Reynolds number flow in single and multiple tube systems," *Trans. ASME*, pp. 1067–1074, Nov. 1950.
[34] A. Žukauskas, "Heat transfer from tubes in crossflow," *Adv. Heat Transf.*, vol. 8, pp. 93–160, 1972.
[35] W. A. Khan, J. R. Culham, and M. M. Yovanovich, "Fluid flow around and heat transfer from an infinite circular cylinder," *J. Heat Transf.*, vol. 127, pp. 785–790, Jul. 2005.
[36] Y. B. Suh, S. Somasundaram, and N. K. Anand, "Remarks on the potential cros flow over tube banks," *J. Appl. Mech.*, vol. 56, pp. 476–479, 1989.
[37] A. Žukauskas and J. Žiugžda, *Heat Transfer of a Cylinder in Crossflow*. New York: Hemisphere, 1985.
[38] R. M. Fand and K. K. Keswani, "A continuous correlation equation for heat transfer from cylinders to air in crossflow for Reynolds numbers from $10^{-2}$ to $2 \times 10^5$," *Int. J. Heat Mass Transf.*, vol. 15, pp. 559–562, 1972.
[39] H. Nakamura and T. Igarashi, "Variation of Nusselt number with flow regimes behind a circular cylinder for Reynolds numbers from 70 30000," *Int. J. Heat Mass Transf.*, vol. 47, pp. 5169–5173, 2004.
[40] Van der Hegge Zijnen, "Modified correlation formulae for heat transfer by natural and forced convection from horizontal cylinders," *Appl. Sci. Res. A*, vol. 6, no. 2–3, pp. 129–140, 1956.

**Waqar Ahmed Khan** is an Associate Professor of mechanical engineering at the National University of Sciences and Technology, Karachi, Pakistan. He has developed several unique analytical models for the fluid flow and heat transfer across single cylinders (circular/elliptical), tube banks, and pin-fin heat sinks to Newtonian and non-Newtonian fluids. His research interests include modeling of forced convection heat transfer from complex geometries, micro-channel heat sinks, thermal system optimization using entropy generation minimization, forced and mixed convection, and conjugate heat transfer in air and liquid cooled applications. He has more than 28 publications in refereed journals and international conferences.

Dr. Khan is a member of ASME, AIAA, and the Pakistan engineering council.

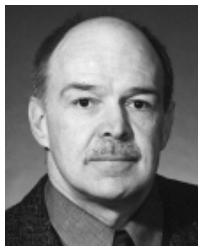

**J. Richard Culham** (M'98) is an Associate Professor of mechanical engineering at the University of Waterloo, Waterloo, ON, Canada. He is the director and a founding member of the Microelectronics Heat Transfer Laboratory. Research interests include modeling and characterization of contacting interfaces and thermal interface materials, development of compact analytical and empirical models at micro- and nano-scales, natural and forced convection cooling, optimization of electronics systems using entropy generation minimization, and the characterization of thermophysical properties in electronics and opto-electronics materials. He has more than 100 publications in refereed journals and conferences in addition to numerous technical reports related to microelectronics cooling.

Prof. Culham is a member of ASME and the Professional Engineers of Ontario.

**M. Michael Yovanovich** received the Sc.D. degree from the Massachusetts Institute of Technology, Cambridge.

He is a Distinguished Professor Emeritus of mechanical engineering at the University of Waterloo, Waterloo, ON, Canada, and is the Principal Scientific Advisor to the Microelectronics Heat Transfer Laboratory. His research in the field of thermal modeling includes analysis of complex heat conduction problems, external and internal natural and forced convection heat transfer from and in complex geometries, and contact resistance theory and applications. He has published more than 350 journal and conference papers, and numerous technical reports, as well as three chapters in handbooks on conduction and thermal contact resistance. He has been a consultant to several North American nuclear, aerospace, and microelectronics industries and national laboratories.

Prof. Yovanovich has received numerous awards for his teaching and his significant contributions to science and engineering. He is the recipient of the AIAA Thermophysics Award and the ASME Heat Transfer Award. He is a Fellow of AAAS, AIAA, and ASME.